AGU PUBLICATIONS

JGR

Journal of Geophysical Research: Atmospheres

RESEARCH ARTICLE
10.1002/2015JD023600

**Key Points:**
- New $Z_e$ parameterization provides a first-order estimation of $Z_e$
- New retrieval has been evaluated with radiative close methods
- $Z_e$ parameterization will allow for more fruitful study of the thin cirrus

**Correspondence to:**
M. Deng,
mdeng2@uwyo.edu

**Citation:**
Deng, M., G. G. Mace, Z. Wang, and E. Berry (2015), CloudSat 2C-ICE product update with a new $Z_e$ parameterization in lidar-only region, *J. Geophys. Res. Atmos.*, *120*, 12,198–12,208, doi:10.1002/2015JD023600.

Received 28 APR 2015
Accepted 14 NOV 2015
Accepted article online 18 NOV 2015
Published online 14 DEC 2015



# CloudSat 2C-ICE product update with a new $Z_e$ parameterization in lidar-only region

**Min Deng[1], Gerald. G. Mace[2], Zhien Wang[1], and Elizabeth Berry[2]**

[1]Department of Atmospheric Science, University of Wyoming, Laramie, Wyoming, USA, [2]Department of Atmospheric Science, University of Utah, Salt Lake City, Utah, USA

**Abstract** The CloudSat 2C-ICE data product is derived from a synergetic ice cloud retrieval algorithm that takes as input a combination of CloudSat radar reflectivity ($Z_e$) and Cloud-Aerosol Lidar and Infrared Pathfinder Satellite Observation lidar attenuated backscatter profiles. The algorithm uses a variational method for retrieving profiles of visible extinction coefficient, ice water content, and ice particle effective radius in ice or mixed-phase clouds. Because of the nature of the measurements and to maintain consistency in the algorithm numerics, we choose to parameterize (with appropriately large specification of uncertainty) $Z_e$ and lidar attenuated backscatter in the regions of a cirrus layer where only the lidar provides data and where only the radar provides data, respectively. To improve the $Z_e$ parameterization in the lidar-only region, the relations among $Z_e$, extinction, and temperature have been more thoroughly investigated using Atmospheric Radiation Measurement long-term millimeter cloud radar and Raman lidar measurements. This $Z_e$ parameterization provides a first-order estimation of $Z_e$ as a function extinction and temperature in the lidar-only regions of cirrus layers. The effects of this new parameterization have been evaluated for consistency using radiation closure methods where the radiative fluxes derived from retrieved cirrus profiles compare favorably with Clouds and the Earth's Radiant Energy System measurements. Results will be made publicly available for the entire CloudSat record (since 2006) in the most recent product release known as R05.

## 1. Introduction

The CloudSat 2C-ICE product describes the vertically resolved microphysical properties of ice clouds [*Deng et al*., 2010, 2013]. The algorithm is a synergetic ice cloud retrieval derived from the combination of the CloudSat radar reflectivity ($Z_e$) and the Cloud-Aerosol Lidar and Infrared Pathfinder Satellite Observation (CALIPSO) lidar attenuated backscatter ($\beta$) using a variational method for deriving profiles of extinction coefficient ($\sigma$), ice water content (IWC), and particle effective radius ($r_e$). The basic methodology is described in *Deng et al*. [2010]. The 2C-ICE product has been evaluated with collocated aircraft in situ measurements and compared with the raDAR/liDAR (DARDAR) [*Delanoë and Hogan*, 2008] and other cloud products [*Deng et al*., 2013]. A recent study [*Matrosov*, 2015] to evaluate retrievals of total ice content in precipitating cloud systems from ground-based operational radar measurements shows that ice water path derived (IWP) from 2C-ICE is in relatively good agreement with IWP from a method developed specifically for thick ice clouds that accounts for ice hydrometers nonsphericity [*Matrosov and Heymsfield*, 2008; *Matrosov and Battaglia*, 2009].

Similar to the 2C-ICE product, the DARDAR cloud product is a synergetic ice cloud retrieval algorithm derived from the combination of the CloudSat radar and CALIPSO lidar using a somewhat contrasting variational method for retrieving profiles of $\sigma$, IWC, and $r_e$ [*Delanoë and Hogan*, 2008]. One of the important differences between 2C-ICE and DARDAR is that 2C-ICE utilizes the fact that clouds in the lidar-only region should have equivalent radar reflectivity factor less than the CloudSat radar sensitivity of about −29 dB*Z*. To exploit this information, 2C-ICE parameterizes $Z_e$ in the lidar-only region which provides an additional constraint on the retrieval and ensures that the numerical inversion can proceed seamlessly through the layer. In *Deng et al*. [2013], this additional weak constraint is shown to provide somewhat superior results in the lidar-only regions compared to DARDAR.

However, parameterizing $Z_e$ in the lidar-only region is not an easy task. In the 2007–2008 version of 2C-ICE [*Deng et al*., 2010] $Z_e$ is parameterized by mapping the attenuated backscattering for a whole granule before the profiling retrieval, assuming that the height distribution of the $Z_e$ below the minimum detectable signals would be similar to what is measured by the ARM Millimeter Cloud Radar (MMCR) [*Moran et al*., 1998]. However, cirrus in the polar regions are much lower and warmer on average than cirrus in the tropics and midlatitudes; therefore, in the 2009–2010 version, the height dependence of $Z_e$ in *Deng et al*. [2010] was

replaced by a temperature dependence for the $Z_e$ parameterization. A discontinuity in retrieved cloud properties was then noted in the lidar-only regions due to the different techniques in $Z_e$ parameterization in the lidar-only region in those two algorithm versions (P. Kablick, personal communication, 2013).

Furthermore, while the simple constraint of a maximum value of $Z_e$ in the lidar-only portion of the layer seems to be useful, using additional ancillary information to provide a more robust parameterization of $Z_e$ has the potential to further constrain the algorithm. Therefore, an improved approach for the $Z_e$ parameterization in the lidar-only region is developed in this paper. The $\sigma$ and $Z_e$ relations has been studied in *Matrosov et al*. [2003] to derive vertical profiles of the visible extinction coefficients in ice clouds from measurements of the radar reflectivity collected by a vertically pointing 35 GHz cloud radar:

$$\sigma\left(\mathrm{m}^{-1}\right) \approx 0.0036\, Z_e^{0.58}\left(\mathrm{mm}^{6}\mathrm{m}^{-3}\right) \tag{1}$$

The uncertainties of radar-based retrievals of cloud visible optical thickness are estimated in *Matrosov et al*. [2003] by comparing retrieval results with optical thicknesses obtained independently from radiometric measurements during the yearlong Surface Heat Budget of the Arctic Ocean field experiment. A negative bias is found due to an inherently low sensitivity of the radar measurements to smaller cloud particles that still contribute noticeably to the cloud extinction.

Another inevitable uncertainty associated with the relation in equation (1) is that the ice particle microphysical properties are derived from an unknowable particle habit that contributes to errors in cross-sectional area and bulk density as a function of particle maximum dimension. While these properties are known to be a function of temperature ($T$) [*Hong et al*., 2007, *Donovan et al*., 2004; *Heymsfield et al*., 2004, 2014], the natural variability of these relationships is presently not known.

The ARM program's Raman Lidar (CARL) [*Goldsmith et al*., 1998] was located side by side with MMCR, at the Southern Great Plains (SGP) site and provides an opportunity for independent measurements of vertical profiles of $\sigma$ and $Z_e$ for optically thin cirrus. The ARM MMCR was a zenith-pointing radar that operated at a frequency of 35 GHz with a vertical sample resolution of 90 m. MMCR could report radar reflectivity of $-50$ dB$Z$ up to 20 km with a mean calibration error of less than 1 dB [*Moran et al*., 1998; *Clothiaux et al*., 1999; *Kollias et al*., 2007]. Such a highly sensitive cloud radar collocated with Raman lidar provides a unique data set that allows for us to develop an improved relationship between $Z_e$ and $\sigma$ for upper troposphere cirrus clouds. In essence, such a relationship brings additional information in the form of ancillary data to the 2C-ICE retrieval algorithm. In the following, we develop and evaluate a new $Z_e$-$\sigma$-$T$ relation for upper tropospheric ice clouds with a goal of improving the 2C-ICE retrieval algorithm.

## 2. New $Z_e$ Parameterization From MMCR and Raman Lidar Observation

### 2.1. Observation Data Set

The Raman lidar at the ARM SGP site transmits a laser wavelength of 355 nm and measures the backscattered elastic return at the same wavelength as well as the water vapor and nitrogen Raman shifted returns at 408 and 387 nm, respectively [*Goldsmith et al*., 1998]. Under cloud-free conditions, the vertical distribution of nitrogen Raman signals is proportional to the nitrogen number density profile, which is well determined by temperature and pressure profiles. Therefore, nitrogen Raman signals can be used to derive the cloud extinction coefficient without assuming a relationship between backscatter and extinction that is typically needed for extinction retrievals from elastic lidar signals [*Ansmann et al*., 1992].

A method similar to that used by *Ansmann et al*. [1992] was applied to CARL measurements to generate a 1000 h cirrus cloud data set including $\sigma$ [*Wang and Sassen*, 2002]. A main limiting factor for cirrus $\sigma$ accuracy derived from the nitrogen Raman is the signal-to-noise ratio. To improve the signal-to-noise ratio of the lidar signal, a 10 min sliding average is applied to the Raman lidar data. During the daytime, the signal in the nitrogen Raman channel is often too noisy for the analysis of the entire cirrus layer. We retrieved the cloud extinction profile from the elastic channel with an average extinction-to-backscatter ratio derived from the Raman channel in the lower cloud portion and/or with the constraint of total optical depth [*Young*, 1995]. Then, extinction profiles from elastic and nitrogen Raman channels are combined to provide the final results. Although, random errors in the retrieved $\sigma$ could be as high as 30% in the data set, the mean bias is small due to effective constraints from nitrogen Raman and molecular elastic signals [*Wang and Sassen*, 2002].

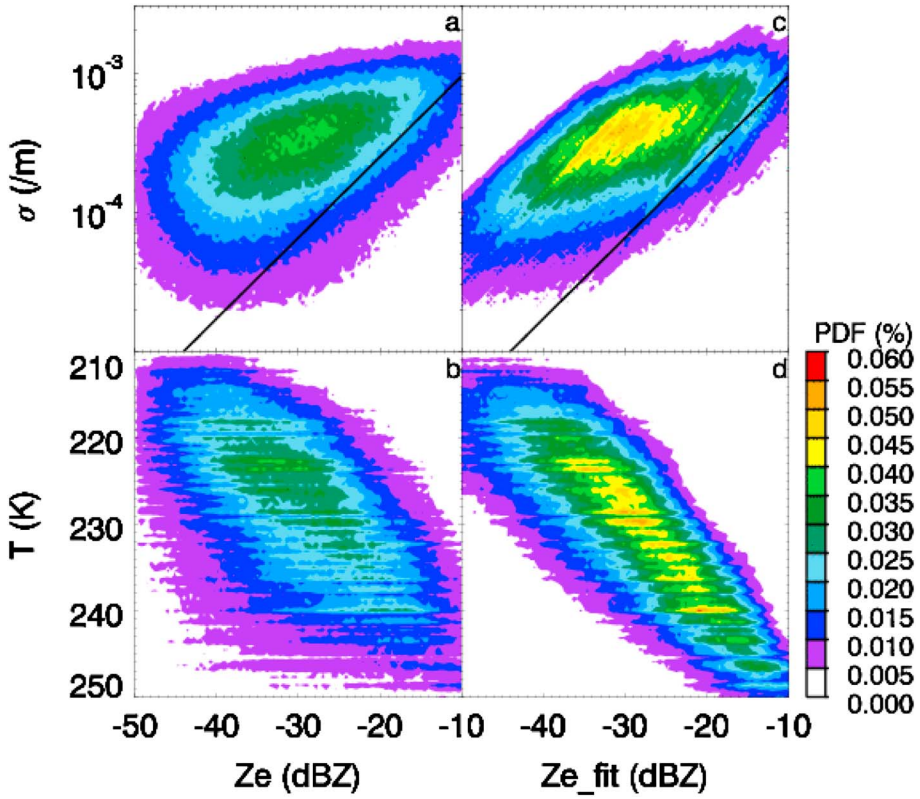


**Figure 1.** (a and b) The PDF of $Z_e$-extinction ($\sigma$) and $Z_e$-$T$ relations from MMCR measurement, Raman lidar, and merged sounding data at ARM SGP site, and the (c and d) parameterized $Z_e$-$\sigma$ and $Z_e$-$T$ relations from equation (2). The black line is derived from the $Z_e$-$\sigma$ relation in *Matrosov et al.* [2003].

The CloudSat Cloud Profiling Radar (CPR) is a 94 GHz nadir-looking radar which measures the power backscattered by clouds as a function of distance from the radar. Other than about 1 dB difference between W and Ka band reflectivity due to the dielectric properties of water [*Doviak and Zrnic*, 1993], which is accounted for in the parameterization, the $Z_e$ is independent of radar wavelength if the hydrometeor's maximum diameter $D$ is much smaller than the radar wavelength and the scattering is described by the Rayleigh approximation.

**Table 1.** List of Comparison Between Parameterized $Z_e$ From Equation (2) and ARM MMCR Observed $Z_e$ in Figure 2a

| MMCR $Z_e$ (dB$Z_e$) | Parameterized $Z_e$ (dB$Z$) Mode/Mean/Standard Deviation | Data Sample (#) |
|---|---|---|
| −46 ± 1 | −44.9/−42.4/8.6 | 25,972 |
| −44 ± 1 | −42.1/−41.2/7.6 | 47,956 |
| −42 ± 1 | −41.2/−40.4/6.6 | 58,875 |
| −40 ± 1 | −39.5/−39.1/6.7 | 86,272 |
| −38 ± 1 | −38.0/−37.3/6.2 | 89,556 |
| −36 ± 1 | −36.0/−35.5/5.5 | 93,027 |
| −34 ± 1 | −34.0/−33.7/5.5 | 97,811 |
| −32 ± 1 | −32.0/−32.0/5.4 | 99,609 |
| −30 ± 1 | −30.0/−30.4/5.5 | 99,941 |
| −28 ± 1 | −28.5/−28.7/5.0 | 97,867 |
| −26 ± 1 | −26.0/−26.8/5.6 | 95,314 |
| −24 ± 1 | −24.0/−25.2/5.5 | 87,660 |
| −22 ± 1 | −22.0/−23.0/5.9 | 83,716 |
| −20 ± 1 | −20.8/−21.6/6.0 | 69,688 |
| −18 ± 1 | −19.1/−20.5/6.3 | 62,508 |
| −16 ± 1 | −17.8/−18.9/6.9 | 53,806 |
| −14 ± 1 | −15.8/−16.9/7.5 | 35,244 |
| −12 ± 1 | −14.0/−14.2/7.5 | 27,084 |

**Table 2.** The Fitted Coefficients of $Z_e$ Parameterization as a Function of Extinction Coefficient and Temperature: $Z_e(\mathrm{dBZ}) = a + b \times \log 10(\sigma) \times \log 10(T) + c \times \log 10(\sigma) \times T + d \times \log 10(\sigma)$, Where $T$ Is in Kelvin and $\sigma$ Is in Per Meter

| Fitting Coefficients | a | b | c | d |
|---|---|---|---|---|
| Fitted value | 27.2890 | 6.42015 | −0.228607 | 51.3835 |

This should be a reasonable assumption for upper troposphere thin cirrus clouds with ice mass equivalent radius smaller than 300 μm [*Wang et al.*, 2005]. The gas attenuation in radar signal decreases as the wavelength increases. This attenuation at MMCR Ka band is smaller compared to that in CloudSat CPR, which is corrected in the CPR data set. Given the cirrus observed by both Raman Lidar and MMCR at SGP site, the sampled cirrus clouds are most likely to be synoptic-scale cirrus than anvil clouds. The attenuation in those profiles should be less than ~0.5 dB mean bias [*Matrosov et al.*, 2004].

Thermodynamic profiles are acquired from the Merged Sounding Data Product provided by the ARM program [*Troyan*, 2011]. This product uses a combination of observations from radiosonde soundings, microwave radiometer-derived water vapor path, surface meteorological instruments, and the European Centre for Medium-Range Weather Forecasts (ECMWF) model and employs a sophisticated scaling/interpolation/smoothing scheme in order to define profiles of the atmospheric thermodynamic state [*Troyan*, 2011]. Because temperature provides a well-known constraint on ice cloud properties [e. g. *Heymsfield et al.*, 2013], we use temperature as an additional parameter to effectively constrain the ice particle habit or particle size distribution variations in the MMCR and Raman Lidar data sets.

Figures 1a and 1b show the probability density functions (PDF) of cirrus clouds in $Z_e/\sigma$ and $Z_e/T$ domains based on the multiyear collocated MMCR and Raman lidar measurements using a 1 min time resolution at the SGP site [*Wang and Sassen*, 2002]. $Z_e$ generally increases with temperature and extinction coefficient. The $Z_e$ ranges from −10 to −50 dB$Z$ over a temperature range from −20 to −60°C. Data sample distribution is listed in 2 dB$Z$ $Z_e$ bins in Table 1. About 50% of data has $Ze$ less than −29 dB$Z$. The overplotted black line in Figures 1a and 1c is derived from equation (1) in *Matrosov et al.* [2003] where a negative bias is found compared to the Raman lidar-MMCR observations in this study.

While $Z_e$ is correlated with $T$ and $\sigma$, there are large deviations existing in both relations. Therefore, parameterizing $Ze$ as single functions of either $T$ or $\sigma$ is not optimal.

### 2.2. New $Z_e$ Parameterization as a Function of $\sigma$ and Temperature

Given the relations shown in Figures 1a and 1b, we used a set of polynomial functions to approximate the relationships between $Z_e$, $\sigma$, and $T$, and found that the following function provides an optimal fit in terms of maximizing correlation coefficients and minimizing standard deviations:

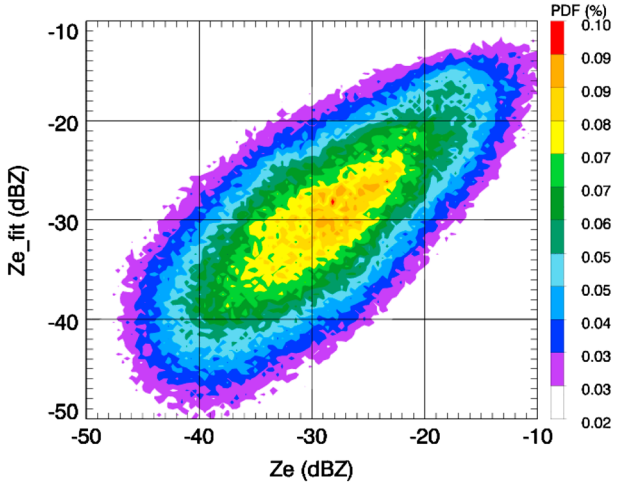


**Figure 2.** Comparison in PDF between $Z_e$ parameterized using equation (2) and the MMCR observed $Z_e$ at the SGP site.

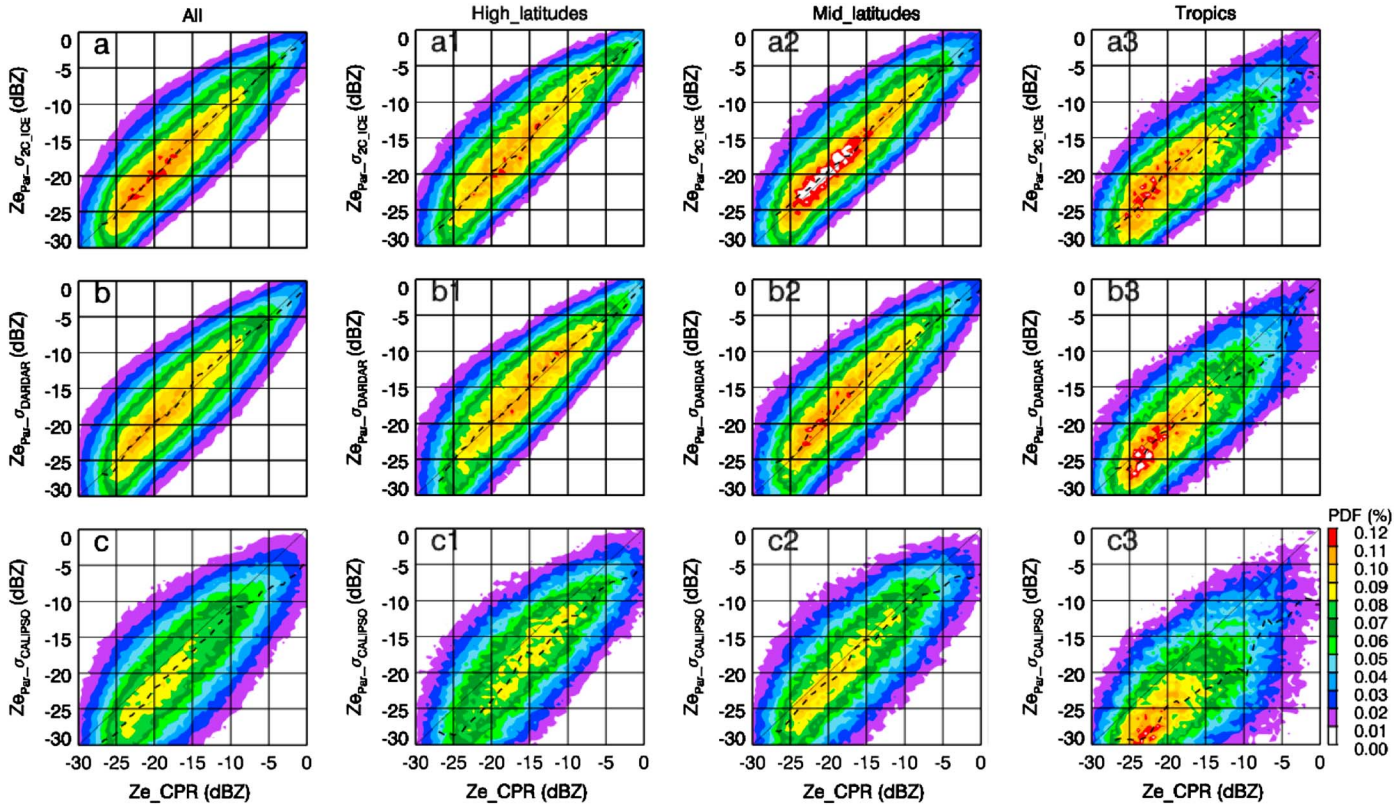


**Figure 3.** Comparison of CloudSat CPR-observed $Z_e$ and parameterized $Z_e$ using equation (2) with $\sigma$ from (a) 2C-ICE, (b) DARDAR, and (c) CALIPSO in the lidar-radar overlap region. The comparisons are separated among (a1, b1, and c1) high latitudes, (a2, b2, and c2) midlatitudes, and (a3, b3, and c3) tropics.

$$Z\ (\mathrm{dBZ}) = a + b \times \log10(\sigma) \times \log10(T) + c \times \log10(\sigma) \times T + d \times \log10(\sigma) \tag{2}$$

where $T$ is in kelvin and $\sigma$ is in per meter. The fitted coefficients are listed in the Table 2. The PDF between fitted $Z_e/T$ and fitted $Z_e/\sigma$ is shown in Figures 1c and 1d. We can see that the relations between the fitted $Z_e$/T and $Z_e/\sigma$ are very similar with observations with certain deviations. The fitted $Z_e$ has a good correlation with observed $Z_e$ ($r = 0.65$) in Figure 2, while the mean bias between the fitted $Z_e$ and the MMCR observed $Z_e$ is less than 3 dB in Table 1. The parameterized $Z_e$ in equation (2) provides a reasonable first-order estimate of $Z_e$ in the lidar-only region for the 2C-ICE retrieval. This parameterization effectively leverages the unique ancillary information provided by many years of collocated Raman lidar and MMCR data. The standard deviation of the parameterized $Z_e$ is substantial (~5–8 dB). This value is designated as the uncertainty of the parameterized $Z_e$ in the lidar-only region in the 2C-ICE retrieval framework.

In the 2C-ICE optimal estimation framework, the $S_\varepsilon$ represents the total measurement error which includes forward model error, random measurement error, and systematic error [*Deng et al.*, 2010]. Given the geographical variation of cirrus clouds and uncertainties in equation (2), the corresponding $Z_e$ error in the lidar-only region is assigned to be ~6 dB. This large error assignment ensures that the parameterized radar reflectivity value provides a weak constraint on the actual retrieved ice cloud properties in this portion of the layer, while the actual information that the radar reflectivity is lower than the minimum detectable by the CPR is retained.

## 3. Evaluation of New $Z_e$ Parameterization

### 3.1. Comparison in the 2C-ICE Lidar-Radar Overlapped Regions

The purpose of parameterizing $Z_e$ from the collocated Raman lidar and MMCR measurements is to provide an additional constraint in the lidar-only region in 2C-ICE retrievals. However, the collocated ARM data used in development of the parameterization includes the so-called radar-lidar overlap region in 2C-ICE because of the high sensitivity of MMCR. Therefore, in the following we compare the parameterized and observed $Z_e$ in the lidar-radar overlapped regions in 2C-ICE as a check on our implementation of the parameterization.

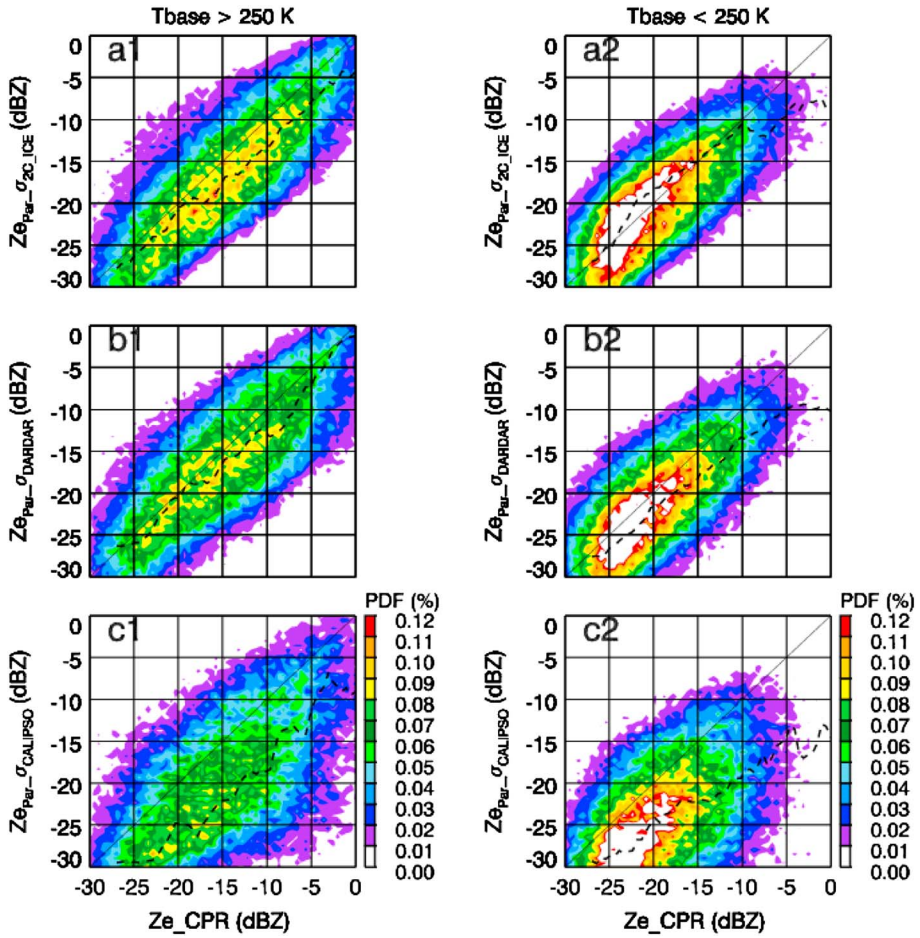


**Figure 4.** Comparison of CloudSat CPR-observed $Z_e$ and parameterized $Z_e$ using equation (2) with $\sigma$ from (a) 2C-ICE, (b) DARDAR, and (c) CALIPSO in tropical ice clouds with cloud base (a1, b1, and c1) warmer than 250 K and (a2, b2, and c2) colder than 250 K in the lidar-radar overlap region.

During the Small Particles in Cirrus [*Deng et al*., 2013] field campaign [*Mace et al*., 2009], the SPEC Inc. Lear Jet flew in coordination with CloudSat and CALIPSO 12 times. The 2C-ICE retrieval along with the DARDAR retrieval and $\sigma$ from CALIPSO were compared with in situ measurements in *Deng et al*. [2013]. For the radar and lidar overlap region, DARDAR and 2C-ICE were found to be in reasonably close agreement with each other and with the in situ measurements. However, flight mean ratios of retrieved $\sigma$ to $\sigma$ derived from in situ measurements using the 2-D stereo (2-DS) [*Lawson et al*., 2006] probe show that retrieved $\sigma$ using algorithms implemented by the CALIPSO team [*Young et al*., 2013] is biased low. This low bias is probably related to the 5 km averaging technique implemented by the CALIPSO team in situations where the cirrus layers have significant horizontal gradients in $\sigma$. Extinction coefficients derived from the CALIPSO algorithms are also found to be biased low compared to synthetic extinction from in situ particle size distributions as reported in *Heymsfield et al*. [2014].

Here, for the 12 granules used in *Deng et al*. [2013], we apply equation (2) with $\sigma$ from the 2C-ICE ($\sigma_{2C\_ICE}$), DARDAR $\sigma$ ($\sigma_{DARDAR}$), and the CALIPSO $\sigma$ ($\sigma_{CALIPSO}$) that is available from the CALIPSO archive and represents the CALIPSO team standard data product. Temperature profiles from the CloudSat ECMWF_AUX product are used to derive the parameterized $Z_e$ in the lidar-radar overlap region, and then we compare the parameterized $Z_e$ with the CloudSat CPR-observed $Z_e$. The comparison results for all locations are shown in Figure 3.

The parameterized $Z_e$ using $\sigma_{2C\_ICE}$ in Figure 3a is very well correlated with CPR-observed $Z_e$ with a correlation coefficient (rr) of 0.85. This good correlation might be expected since the 2C-ICE retrieval has already assumed the $Z_e$ parameterization in the lidar-only region although not in the overlap region. The $\sigma_{DARDAR}$

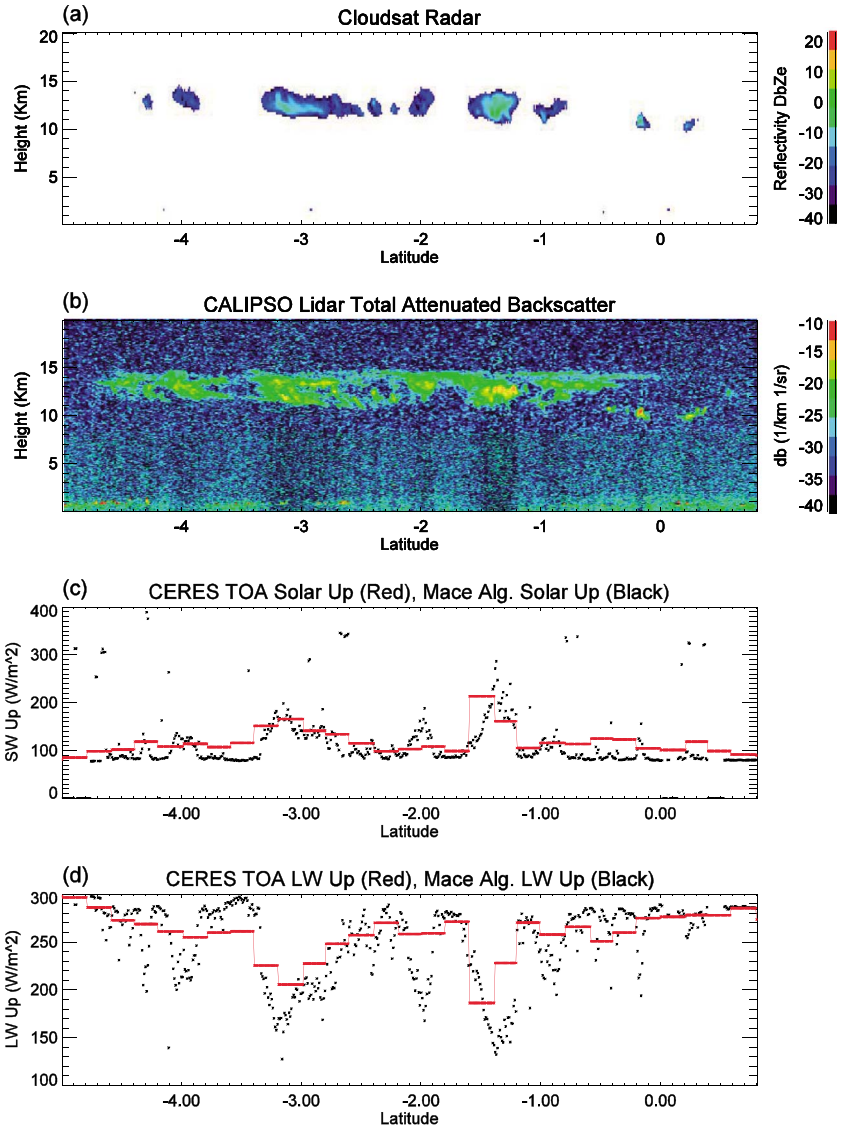


**Figure 5.** Comparison of radiative fluxes calculated using 2C-ICE results that include the new $Z_e$ constraints discussed in the text with flux measurements collected by CERES on 3 August 2007 over south of the Bay of Bengal. Measured (a) CloudSat radar reflectivity and (b) CALIOP attenuated backscatter and the calculated upward (c) shortwave and (d) longwave flux comparison using the new $Z_e$ constraint in the 2C-ICE retrieval (dots) with CERES (red lines).

is retrieved independently from CALIPSO and CPR data at the University of Lille in France, although the parameterized $Z_e$ using $\sigma_{DARDAR}$ in Figure 3b is also well correlated with CPR-observed $Z_e$ (rr = 0.81). The mean biases between the parameterized $Z_e$ with $\sigma_{2C\_ICE}$ and $\sigma_{DARDAR}$ and the CPR-observed $Z_e$ are small.

Although the $\sigma$ ($\sigma_{CALIPSO}$) is calculated independently in the CALIPSO level 2 product [*Young and Vaughan*, 2009] from Cloud-Aerosol Lidar with Orthogonal Polarization (CALIOP) only, the parameterized $Z_e$ using $\sigma_{CALIPSO}$ is also correlated with CPR-observed $Z_e$ (rr = 0.68). However, the parameterized $Z_e$ with $\sigma_{CALIPSO}$ has a negative bias compared to CPR-observed $Z_e$ and the parameterized $Z_e$ with $\sigma_{2C\_ICE}$ and $\sigma_{DARDAR}$, since $\sigma_{CALIPSO}$ is smaller compared to $\sigma_{2C\_ICE}$ and $\sigma_{DARDAR}$.

Having been derived from the broadest possible range of dynamics, aerosol, and thermodynamic conditions, we expect that the ice clouds to which we apply the 2C-ICE algorithm are much more diverse in terms of their microphysical properties than the cirrus clouds from the ARM SGP site. Therefore, the comparison of CloudSat CPR-observed $Z_e$ and parameterized $Z_e$ in the lidar and radar overlapped regions is separated among high

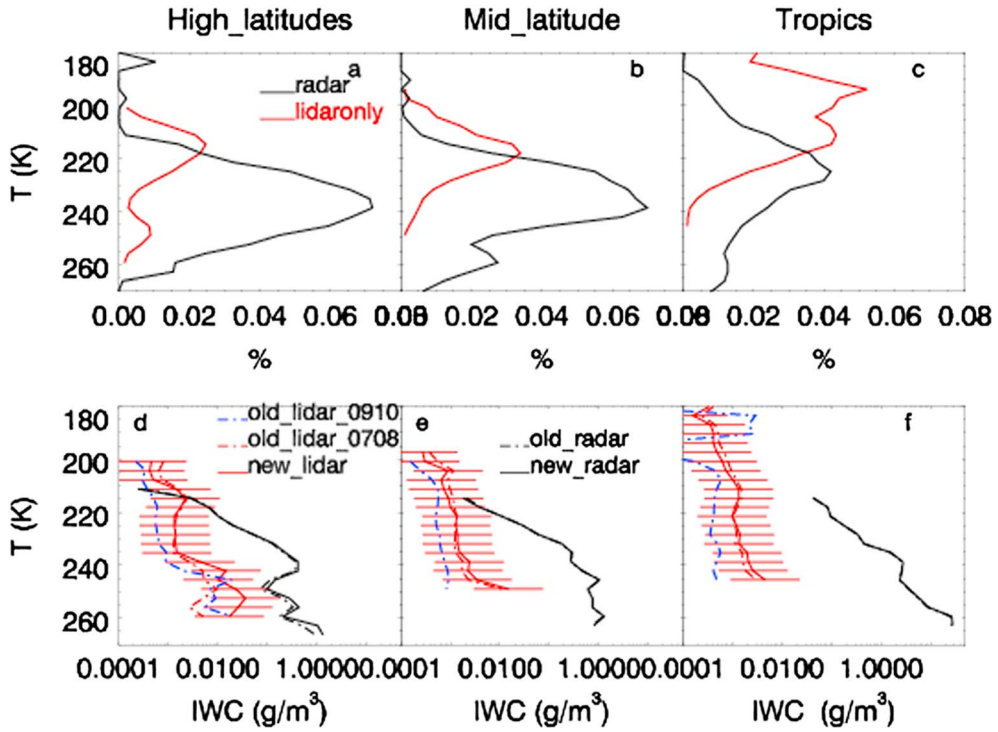


**Figure 6.** (a–c) Ice cloud frequency distributions as a function of temperature in the lidar-only (red) and the radar regions (black) for high latitude (Figure 6a), midlatitude (Figure 6b), and tropics (Figure 6c) regions. (d–f) Mean IWC as a function of temperature in lidar (red) and radar (black) regions for corresponding latitude bands. The solid red lines show the mean and standard deviation of IWC from the lidar-only region from the new $Z_e$ constraints discussed in the text. The dashed lines show previous versions (2007–2008 version in red; 2009–2010 version in blue) that include an erroneous discontinuity that is now superseded by the new work reported on here.

latitudes, midlatitudes, and tropics in Figure 3. We find that the parameterized $Z_e$ from the 2C-ICE extinction is generally close to the CloudSat CPR observations except for the clouds with large extinction in the tropics in Figure 3a. Given the strong correlation between the distance of anvil clouds to their parent convective core edge and the cloud base temperature in the recent study of tropical anvil clouds [*Deng et al.*, 2015], we further separate the comparison for tropical ice cloud layers with cloud bases warmer or colder than 250 K in Figure 4. The ice clouds with cloud base colder than 250 K represent the cirrus that is generally far away from a convective core and have less influence from convection, and therefore have different properties from those with cloud base warmer than 250 K, which are likely often associated with outflow from convection, hereafter anvil clouds. Figure 4 shows that the parameterized $Z_e$ of anvil clouds from 2C-ICE extinction is slightly biased low by about 2–3 dB to the CloudSat CPR observations. This bias might be related to particle size differences or other microphysical assumptions, but the comparison is still within the standard deviation range (±6 dB$Z$) of the $Z_e$ given in Table 1.

### 3.2. Evaluation of Retrieved 2C-ICE Through Radiation Closure

The newly developed $Z_e$ parameterization in the lidar-only region has been applied to 2C-ICE from 2007 to 2010. Radiative properties and profiles of radiative fluxes along the CloudSat track can be derived using a suite of techniques that were initially developed and applied to a similar suite of ground-based remote sensors [*Mace et al.*, 2006a, 2006b; *Mace and Benson*, 2008] and to A-Train data [*Mace*, 2010; *Berry and Mace*, 2014]. In *Berry and Mace* [2014], vertically resolved ice water content, ice particle effective radius, and extinction coefficient profiles from 2C-ICE were used in place of the more primitive cirrus retrievals of the earlier algorithms, and the calculated Top of the atmosphere (TOA) fluxes were compared to Clouds and the Earth's Radiant Energy System (CERES) fluxes to provide some understanding of the quality of the cloud properties using TOA radiative closure [*Berry and Mace*, 2014].

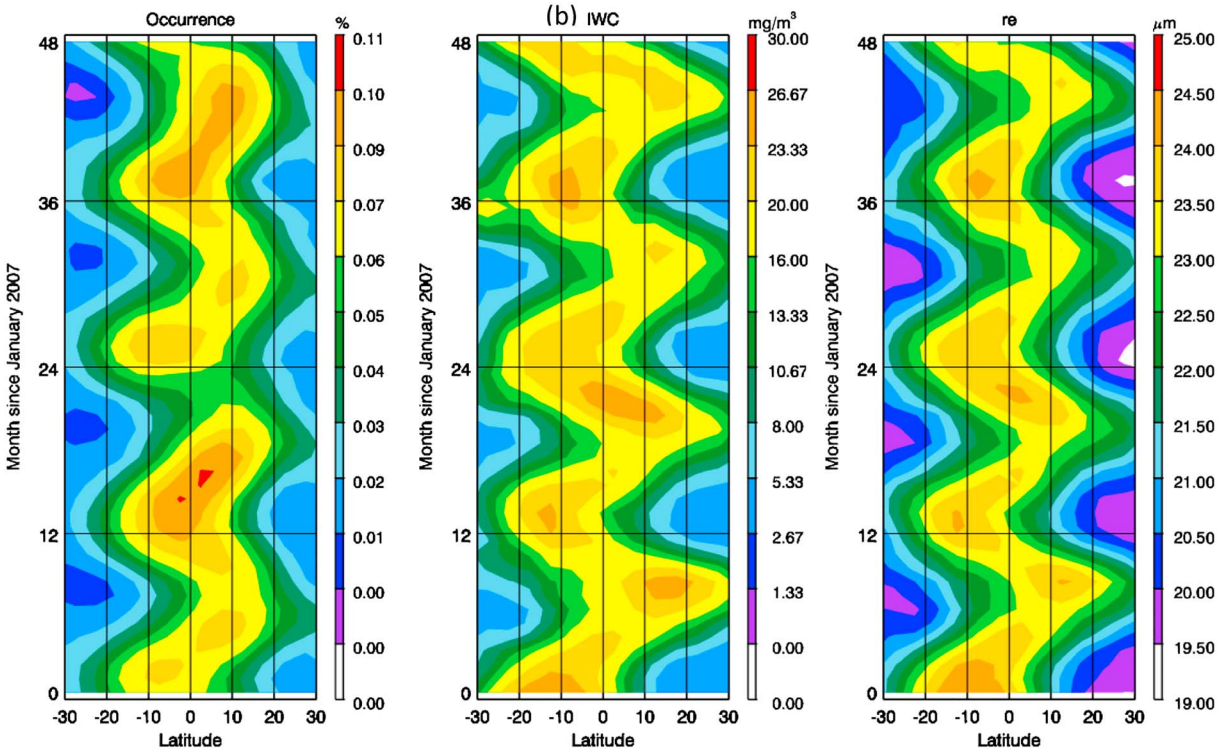


**Figure 7.** The monthly zonal mean occurrence, mean $r_e$, and IWC of ice at 210 K ± 1.5 K since January 2007.

One case study for a relatively thin ice cloud layer on 3 August 2007 is selected to illustrate a radiative fluxes comparison between calculations with the updated 2C-ICE retrieval and CERES measurements in Figure 5. This cirrus cloud layer is above 10 km and is mainly observed by the CALIPSO lidar. Our derived values generally compare well with CERES radiative fluxes which are shown in red in Figures 5c and 5d. Given the optically thin nature of this layer over a relatively dark marine background, only approximately 100 W m$^{-2}$ of solar radiation is reflected. The outgoing longwave radiation is about 250 W m$^{-2}$. Errors in 2C-ICE algorithm translate into errors in the radiative property profiles and ultimately to the radiative fluxes. However, we find that the solar and IR fluxes derived from 2C-ICE track the CERES data reasonably well. This is especially evident in the region near −3 and −1.5 south latitude, where variations in the microphysics drive variations in the fluxes that provide a nice match between CERES and 2C-ICE. From the case study here and monthly averaged data analysis in *Berry and Mace*, 2014, errors in the monthly-averaged cloud radiative effects are assumed to be on the order of 5–10 W m$^{-2}$.

## 4. Discussion and Conclusion

To evaluate the impact of the new $Z_e$ parameterization in the lidar-only region of the 2C-ICE product, we compare the new 2C-ICE results with previous versions of the algorithm in Figure 6 for the lidar-only region and the radar region, which includes the radar and lidar overlap region and radar-only regions. The PDFs of ice clouds in the lidar-only and radar regions for high latitudes (60°–90°), midlatitudes (30°–60°), and tropics (30°S–30°N) in Figures 6a–6c show that the fraction of lidar-only region exceeds that of radar region above 220 K in the tropics.

We can see that the retrieved IWC with new $Z_e$ parameterization is very close to the old 2007–2008 version except for the lidar-only region warmer than 240 K in high latitudes, while IWC in the radar region is almost the same. For 2009–2010 data, the IWC in the lidar-only region in the new 2C-ICE data that uses the more accurate $Z_e$ parameterization (Equation (2)) tends to be larger than the IWC in the older now obsolete version by about a factor of 2 to 5, while IWC in the radar region is almost unchanged. This change in the lidar-only region is within the standard deviation of IWC. The IWC in the lidar-only region is order smaller than that found in the radar region, which indicates that only a small portion of the total ice mass in the vertical column

tends to exist in lidar-only region, and from a mass perspective it is relatively unimportant to global atmospheric ice mass budget statistics [*Li et al*., 2012]. However, the IWC that exists in the lidar-only region is very important to understand variations in cirrus cloud radiative effects [*Berry and Mace*, 2014; *Comstock et al*., 2002, 2013; *Sassen and Comstock*, 2001].

As a brief example of the richness of this data set, Figure 7 shows the tropical monthly zonal mean occurrence, mean $r_e$, and IWC of ice at 210 K ± 1.5 K since January 2007. The locations of maximum cirrus occurrence frequency at a temperature of 210 K transit from 10°S in January to 10°N in July on a well-defined annual cycle. The latitudinal migration of ice cloud occurrence and microphysical properties is well correlated with solar insolation and tropical convection. However, the corresponding values of $r_e$ and IWC are better correlated with each other than with the occurrence frequency. Overall, the Southern Hemisphere, southward of 20°S, demonstrates a minimum in ice cloud occurrence during boreal summer associated with the descending branch of the Hadley Cell. It is interesting to note both annual mean asymmetry in the hemispheres and interannual variability in cirrus occurrence and zonal mean properties. We expect that improvements to the 2C-ICE algorithm due to the $Z_e$ parameterization will allow for more fruitful study of the thin cirrus observed only by the CALIPSO lidar. The new 2C-ICE product has been used for recent studies of cirrus cloud properties and their radiative effect [*Huang et al*., 2015].

In summary, utilizing the capability of ARM Raman lidar to observe $\sigma$ and the high sensitivity of the ARM MMCR to observe thin cirrus, a new parameterization relating $Z_e$ and $\sigma$ for the 2C-ICE lidar-only region has been developed. The parameterized $Z_e$ agrees well with CloudSat observed $Z_e$ in the 2C-ICE lidar and radar overlapped region. Results from the updated 2C-ICE algorithm with the new $Z_e$ parameterization have been examined with radiation closure methods. The resulting radiative fluxes compare favorably with CERES measurement. This new $Z_e$ parameterization utilizes $\sigma$ in addition to temperature, rather than just height, and is now more suitable for global ice cloud retrievals as compared to earlier approaches. The updated 2C-ICE product with the new $Z_e$ parameterization removes a discontinuity in retrieved cloud properties which has been reported in the lidar-only regions due to different techniques used relating $Z_e$ and $\sigma$ in the lidar-only region.

**Acknowledgments**

The ARM Raman lidar data and MMCR data were acquired from ARM data archive. The A-Train data are acquired from CloudSat Data Processing Center at Colorado State University (http://www.cloudsat.cira.colostate.edu/). DARDAR data are downloaded from ICARE Data and Services Center (http://www.icare.univ-lille1.fr/drupal/projects/dardar). CALIPSO data are downloaded from NASA Atmospheric Science Data Center (https://eosweb.larc.nasa.gov/project/calipso/calipso_table). We would like to thank the engineers, technicians, and scientists for the high-quality and well-documented data. This work is supported by NASA though contract issued by Jet Propulsion Laboratory. The authors also want to thank A. Heymsfield and S.Y. Matrosov for their fruitful comments and anonymous reviewers for their thoughtful help to clarify the manuscript.

## References

Ansmann, A., U. Wandinger, M. Riebesell, C. Weitkamp, and W. Michaelis (1992), Independent measurement of extinction and backscatter profiles in cirrus clouds by using a combined Raman elastic-backscatter lidar, *Appl. Opt.*, *31*, 7113–7131.

Berry, E., and G. G. Mace (2014), Cloud properties and radiative effects of the Asian summer monsoon derived from A-Train data, *J. Geophys. Res. Atmos.*, *119*, 9492–9508, doi:10.1002/2014JD021458.

Clothiaux, E. E., K. P. Moran, B. E. Martner, T. P. Ackerman, G. G. Mace, T. Uttah, J. H. Mather, K. B. Widener, M. A. Miller, and D. J. Rodriguez (1999), The Atmospheric Radiation Measurement program cloud radars: Operational modes, *J. Atmos. Oceanic Technol.*, *16*, 819–827.

Comstock, J. M., T. P. Ackerman, and G. G. Mace (2002), Ground-based lidar and radar remote sensing of tropical cirrus clouds at Nauru Island: Cloud statistics and radiative impacts, *J. Geophys. Res.*, *107*(D23), 4714, doi:10.1029/2002JD002203.

Comstock, J. M., A. Protat, S. A. McFarlane, J. Delanoe, and M. Deng (2013), Assessment of uncertainty in cloud radiative effects and heating rates through retrieval algorithm differences: Analysis using 3 years of ARM data at Darwin, Australia, *J. Geophys. Res. Atmos.*, *118*, 4549–4571, doi:10.1002/jgrd.50404.

Delanoë, J., and R. J. Hogan (2008), A variational scheme for retrieving ice cloud properties from combined radar, lidar, and infrared radiometer, *J. Geophys. Res.*, *113*, D07204, doi:10.1029/2007JD009000.

Deng, M., G. G. Mace, Z. Wang, and H. Okamoto (2010), Tropical Composition, Cloud and Climate Coupling Experiment validation for cirrus cloud profiling retrieval using CloudSat radar and CALIPSO lidar, *J. Geophys. Res.*, *115*, D00J15, doi:10.1029/2009JD013104.

Deng, M., G. G. Mace, Z. Wang, and R. P. Lawson (2013), Evaluation of several A-Train ice cloud retrieval products with in situ measurements collected during the SPARTICUS campaign, *J. Appl. Meteorol. Climatol.*, *52*, 1014–1030.

Deng, M., G. G. Mace, Z. Wang (2015), Anvil productivity of tropical deep convective Clusters and their regional differences, *J. Atmos. Sci.*, under review.

Donovan, D. P., M. Quante, I. Schlimme, and A. Macke (2004), Use of equivalent spheres to model the relation between radar reflectivity and optical extinction of ice cloud particles, *Appl. Opt.*, *43*, 4929–4940, doi:10.1364/AO.43.004929.

Doviak, R. J., and D. S. Zrnic (1993), *Doppler Radar and Weather Observation*, *Nature*, 562 pp., Academic Press, Orlando.

Goldsmith, J. E. M., F. H. Blair, S. E. Bisson, and D. D. Turner (1998), Turn-key Raman lidar for profiling atmospheric water vapor, clouds, and aerosols, *Appl. Opt.*, *37*, 4979–4990.

Heymsfield, A. J., C. G. Schmitt, A. Bansemer, D. Baumgardner, E. M. Weinstock, J. T. Smith, and D. Sayres (2004), Effective ice particle densities for cold anvil cirrus, *Geophys. Res. Lett.*, *31*, L02101, doi:10.1029/2003GL018311.

Heymsfield, A. J., C. Schmitt, and A. Bansemer (2013), Ice cloud particle size distributions and pressure-dependent terminal velocities from in situ observations at temperatures from 0° to −86 °C, *J. Atmos. Sci.*, *70*, 4123–4154, doi:10.1175/JAS-D-12-0124.1.

Heymsfield, A., D. Winker,, M. Avery, M. Vaughan, G. Diskin, M. Deng,; V. Mitev, and R. Matthey (2014), Relationships between ice water content and volume extinction coefficient from in situ observations for temperatures from 0° to −86 °C: Implications for spaceborne lidar retrievals, *J. Appl. Meteorol. Climatol.*, *53*, 479–505.

Hong, G. (2007), Radar backscattering properties of nonspherical ice crystals at 94 GHz, *J. Geophys. Res.*, *112*, D22203, doi:10.1029/2007JD008839.

Huang, L., J. H. Jiang, Z. Wang, H. Su, M. Deng, and S. Massie (2015), Climatology of cloud water content associated with different cloud types observed by A-Train satellites, *J. Geophys. Res. Atmos.*, *120*, 4196–4212, doi:10.1002/2014JD022779.

Kollias, P., E. E. Clothiaux, M. A. Miller, E. P. Luke, K. L. Johnson, K. P. Moran, K. B. Widener, and B. A. Albrecht (2007), The Atmospheric Radiation Measurement Program cloud profiling radars: Second-generation sampling strategies, processing and cloud data products, *J. Atmos. Oceanic Technol.*, *24*, 1199–1214.

Lawson, R. P., D. O'Connor, P. Zmarzly, K. Weaver, B. Baker, and Q. Mo (2006), The 2D-S (stereo) probe: Design and preliminary tests of a new airborne, high-speed, high-resolution particle imaging probe, *J. Atmos. Oceanic Technol.*, *23*, 1462–1477.

Li, J.-L., F. D. E. Waliser, W.-T. Chen, B. Guan, T. Kubar, G. Stephens, H.-Y. Ma, M. Deng, L. Donner, C. Seman, and L. Horowitz (2012), An observationally-based evaluation of cloud ice water in CMIP3 and CMIP5 GCMs and contemporary reanalysis using contemporary satellite data, *J. Geophys. Res.*, *117*, D16105, doi:10.1029/2012JD017640.

Mace, G. G. (2010), Cloud properties and radiative forcing over the maritime storm tracks of the North Atlantic and Southern Ocean as derived from A-Train, *J. Geophys. Res.*, *115*, D10201, doi:10.1029/2009JD012517.

Mace, G. G., and S. Benson (2008), The vertical distribution of cloud radiative forcing at the SGP ARM Climate Research Facility as revealed by 8-years of continuous data, *J. Clim.*, *21*, 2591–2610.

Mace, G. G., et al. (2006a), Cloud radiative forcing at the ARM Climate Research Facility: 1. Technique, validation, and comparison to satellite derived diagnostic quantities, *J. Geophys. Res.*, *111*, D11S90, doi:10.1029/2005JD005921.

Mace, G. G., et al. (2006b), Cloud radiative forcing at the Atmospheric Radiation Measurement Program Climate Research Facility: 1. Technique, validation, and comparison to satellite-derived diagnostic quantities, *J. Geophys. Res.*, *111*, D11S90, doi:10.1029/2005JD005921.

Mace, J., E. Jensen, G. McFarquhar, J. Comstock, T. Ackerman, D. Mitchell, X. Liu, and T. Garrett (2009), SPartICus: Small particles in cirrus science and operations plan, Publications (E). Paper 33.

Matrosov, S. V. (2015), The use of CloudSat data to evaluate retrievals of total ice content in precipitating cloud systems from ground-based operational radar measurements, *J. Appl. Meteorol. Climatol.*, *54*, 1663–1674, doi:10.1175/JAMC-D-15-0032.1.

Matrosov, S. Y., and A. Battaglia (2009), Influence of multiple scattering on CloudSat measurements in snow: A model study, *Geophys. Res. Lett.*, *36*, L12806, doi:10.1029/2009GL03.

Matrosov, S. Y., and A. J. Heymsfield (2008), Estimating ice content and extinction in precipitating cloud systems from CloudSat radar measurements, *J. Geophys. Res.*, *113*, D00A05, doi:10.1029/2007JD009633.

Matrosov, S. Y., M. D. Shupe, A. J. Heymsfield, and P. Zuidema (2003), Ice cloud optical thickness and extinction estimates from radar measurements, *J. Appl. Meteorol.*, *42*, 1584–1597, doi:10.1175/1520-0450.

Matrosov, S. Y., T. Uttal, and D. A. Hazen (2004), Evaluation of radar reflectivity-based estimates of water content in stratiform marine clouds, *J. Appl. Meteorol.*, *43*, 405–419.

Moran, K. P., B. E. Martner, R. A. Kropfli, M. J. Post, D. C. Welsh, and K. B. Widener (1998), An unattended cloud-profiling radar for use in climate research, *Bull. Am. Meteorol. Soc.*, *79*, 443–455.

Sassen, K., and J. M. Comstock (2001), A midlatitude cirrus cloud climatology from the facility for Atmospheric Remote Sensing. Part III: Radiative properties, *J. Atmos. Sci.*, *58*, 2113–2127.

Troyan, D. (2011), Sonde adjust value-added product technical report, U.S. Department of Energy. DOE/SC-ARM-TR-102. [Available at http://www.arm.gov/publications/tech_reports/doe-sc-arm-tr-102.pdf.]

Wang, Z., and K. Sassen (2002), Cirrus cloud microphysical property retrieval using lidar and radar measurements: II midlatitude cirrus microphysical and radiative properties, *J. Atmos. Sci.*, *59*, 2291–2302.

Wang, Z., G. M. Heymsfield, L. Li, and, A. J. Heymsfield (2005), Retrieve optically thick ice cloud microphysical properties by using airborne dual-wavelength radar measurements. *J. Geophys. Res.*, *110*, D19201, doi:10.1029/2005JD005969.

Young, S. A. (1995), Analysis of lidar backscatter profiles in optically thin clouds, *Appl. Opt.*, *34*, 7019–7031.

Young, S. A., and M. A. Vaughan (2009), The retrieval of profiles of particulate extinction from Cloud Aerosol Lidar Infrared Pathfinder Satellite Observations (CALIPSO) data: Algorithm description, *J. Atmos. Oceanic Technol.*, *26*, 1105–1119.

Young, S. A., M. A. Vaughan, R. E. Kuehn, and D. M. Winker (2013), The retrieval of profiles of particulate extinction from Cloud-Aerosol Lidar and Infrared Pathfinder Satellite Observations (CALIPSO) data: Uncertainty and error sensitivity analyses, *J. Atmos. Oceanic Technol.*, *30*, 395–428, doi:10.1175/JTECH-D-12-00046.1.